Chapter 6

Analysis of Various Energy Storage Systems for Variable Speed Wind Turbines

Youngil Kim and Robert J. Harrington

Additional information is available at the end of the chapter

http://dx.doi.org/10.5772/intechopen.72294

Abstract

During the high penetration of wind power, wind turbines can affect power quality directly due to an unstable and intermittency source. Voltage fluctuations, harmonics, and voltage drops might be factors in this environment. Energy storage systems (ESSs) with variable speed wind turbines (VSWTs) as a permanent magnetic synchronous generator (PMSG) and a doubly fed induction generator (DFIG) could be a solution to improve the power quality from the "variability" of wind power. This chapter investigates the proposed system, which comprises a hybrid ESS for the VSWT. It analyzes the ability of various ESSs (B, SC, and EDLC) based on VSWTs with various ESSs for power quality in terms of average THD (%) specified in reference to IEEE std-519-1992 and IEC 61400-21-Ed.2.0. In addition, this chapter investigates the DFIG with hybrid energy storage systems (Li ion battery and super capacitor ESS) for the economic evaluation in terms of payback time. The simulation results have been verified by a power system computer-aided design/electromagnetic transients direct current (PSCAD/EMTDC) to demonstrate the system performance under different scenarios.

Keywords: VSWT, hybrid ESS, total harmonic distortion, power quality, payback time, PSCAD/EMTDC

1. Introduction

The DOE's 2009 Annual Energy Outlook projected energy accumulation in the USA. The report describes that the future growth of domestic electric energy will increase by 26% for electricity sector by 2030. This might not only require additional generation capacity of 259 GW but also forecast to increase as 1.7% of total installed capacity until 2030 [1, 2]. Variable speed wind turbine prefers to the conventional operation to extract the maximum power from the unstable wind generation. Since speed of wind turbine is nonconstant, the generator should

be controlled by the power electronic circuit. Two variable speed wind turbines (VSWTs) on a principle of power electronics could be classified as DFIGs and PMSGs [3, 4].

DFIG-based wind turbine is a wound rotor induction generator. It consists of three-phase windings on the rotor and stator. The stator winding of the wind turbine is directly connected to the grid winding, while the rotor winding of the generator is fed by variable frequency bidirectional back-to-back PWM based on the voltage source converter, which consists of rotor side converter (RSC) and grid side converter (GSC). It has typically about 30% of nominal generator power [3, 4]. The synchronous machine has the ability to provide its own excitation on the rotor. Such excitation may be obtained by means of either a current carrying winding or permanent magnets (PMs) [5]. PM excitation avoids the field current supply or reactive power compensation facilities [2, 6–8]. PMSG is a permanent magnet synchronous machine with its stator windings connected to the grid through a frequency converter. Signal frequency is generated via the pulse width modulation (PWM) with the DC link of back-to-back voltage source converters (VSCs) consisting of machine side converter and grid side converter [9, 10].

There are several state-of-the-art technologies on wind power and energy storage to improve power quality and stability by optimal control of ESS [11–17], hybrid ESS [18, 19], and renewable forecasting modeling [20, 21]. It is widely popularized that an elaborately optimal control strategy for ESS is to smooth wind power fluctuations for the renewable energy [11–14]. Two configurations of DFIG-BESS for internal and external controllers have improved the capability integrated to the grid [15]. In [16], an optimal control scheduling was considered on the variable smoothing time constant and charging/discharging of power limits, which is to mitigate the wind power fluctuations, while extending the battery life cycle of the BESS. A control strategy of the ESS in the wind farm focused an open-loop optimal control scheme is to incorporate the operating limits of BESS based on the forecasted wind condition [17]. The author [18] introduced the hybrid energy storage system (HESS) to overcome the fast PV-wind power generation fluctuations by smart scheduling, which has a statistical approach for the capacity distribution of the HESS. However, they did not demonstrate real-time simulation with few limited cases. The control and energy management of the hybrid ESS (battery and super capacitor) with DFIG has coordinated the power flows and load demand [19]. Prediction scheme of wind power generation connected to battery ESS developed by using numeric weather prediction model which required to the input as detailed wind information [20]. However, they did not smooth to power variation scheme in this chapter. Energy management system of flywheel ESS used to fuzzy logic for two optimized models as constraint condition and determine optimization objective to control of FESS [21].

2. Configuration of the hybrid ESS of the variable speed wind turbines

The configuration of the HYESS-DFIG is illustrated in **Figure 1(a)**. DFIG is a variable speed wind turbine with a partial scale power converter in the rotor circuit. The main objective of the

http://dx.doi.org/10.5772/intechopen.72294

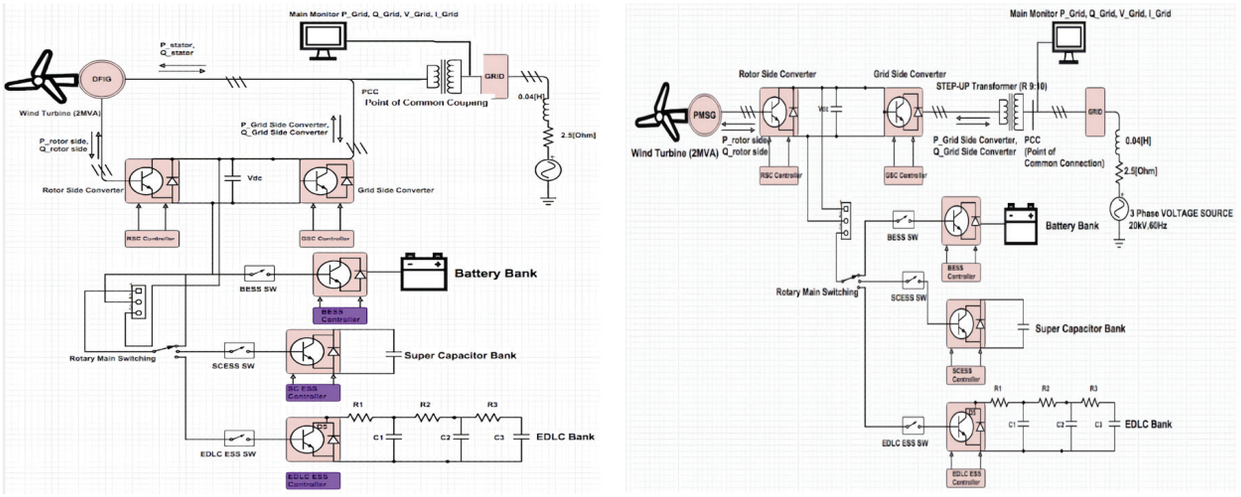

Figure 1. Block diagram of the hybrid energy storage system connected to the configuration variable speed wind turbines: (a) DFIG (left) and (b) PMSG (right).

Generated Rated MVA	2 [MVA]
Machine rated angular mechanical speed	125.667 [rad/s]
Rotor radius	44 [m]
Rotor area	2124 [m^2]
Air density	1.229 [kg/m^3]
Gear box efficiency	0.97 [P.U]
Gear ratio-machine/Turbine	60
Equation for power coefficient	Mode 2

Table 1. PSCAD/EMTDC parameters of the wind turbine for DFIG, PMSG in the proposed systems [23].

RSC controller is to regulate active power (Ps) and reactive power (Qs) of the stator side independently, while the GSC controller is to keep the constant DC voltage (V_{dc}) to adjust reactive power (Qg) of the GSC, which transfers from the grid side [22]. **Figure 1(b)** describes that PMSG which is a variable speed wind turbine with a direct-drive generator connected to the grid through a full-scale power converter [2, 6]. Three different ESS such as battery (B), super capacitor (SC), and electrical dual layer capacitor (EDLC) were introduced in **Figure 1**. Each ESS controller comprised bank, inductance and two-quadrant DC/DC converter connected to the DC link as illustrated in **Figure 1**. Two DC/DC converter design includes two insulated gate Bi-polar junction transistors (IGBTs) diode switches as S1 and S2. To compare two different VSWTs, that is, DFIG and PMSG, three-phase voltage sources are employed at 20 kV, 60 Hz, 0.04 H, and 2.5 Ω, and PSCAD parameter of the wind turbine given in **Table 1**.

2.1. Model of the wind turbines

Variable speed wind turbine could be mathematically described by the follows (1), (2), (3). A wind turbine extracts kinetic energy ($P_{wind(kin)}$) from the swept area (Area) of the blades. The power of the airflow ($P_{airflow}$) is given by [3, 24]:

$$P_{air} = \frac{1}{2} \cdot \rho \cdot Area \cdot v^3 \tag{1}$$

where ρ, *Area*, *v* is the symbol of air density (approximately 1.225 kg/m^3), swept area of rotor (m^2), upwind free wind speed (m/s), respectively.

The wind power ($P_{wind(kin)}$) transferred to the rotor of VSWT could be expressed by

$$P_{wind(kin)} = C_{pt}(\lambda, \beta) \cdot \frac{1}{2} \cdot \rho \cdot Area \cdot v^3 \tag{2}$$

where $C_{pt}(\lambda, \beta)$ is a power coefficient, λ is a function of tip speed ratio , and β is pitch angle. Wind turbines are characterized by their aerodynamic torque or turbine torque as Ta [3, 24, 25]:

$$Ta = \frac{C_{pt}(\lambda, \beta) \frac{1}{2} \cdot \rho \cdot Area \cdot v^3}{\Omega_t} \tag{3}$$

where A is the maximum value of C_{pt} defined by the Betz limit, which a turbine can never extract more than 59.3% of the power from an air stream [21, 25]. In reality, wind turbine rotors have maximum C_p values in the range 25–45% [7].

2.2. Park's model of the VSWT

For our proposed system, the Park's model was used in VSWT (DFIG and PMSG) [3]. The voltage equations in the d, q axes-frame are given as follows [4, 5, 22, 26]:

$$V_d = \frac{d\phi_d}{dt} - \omega_r \phi_q + R_a I_d \tag{4}$$

$$V_q = \frac{d\phi_q}{dt} + \omega_r \phi_d + R_a I_q \tag{5}$$

$$\omega_r = \frac{d\theta}{dt} \tag{6}$$

$$\theta = \int_0^t \omega_r dt + \theta_0 \tag{7}$$

$\phi_d, \phi_q, I_d, I_q, V_d, V_q$ are the stator fluxes, current and voltage of the d and q components; R_a is the stator resistance; ω_r is the rotor speed in electrical [radians/s]. The general Park's

model is used to explain about the control scheme of an induction machine. The equation of voltage vector in the DFIGs is expressed as follows [4, 5, 22, 26]:

$$V_s = R_s i_s + \frac{d\phi}{dt} + j\omega_s \varnothing_s \tag{8}$$

$$V_r = R_r i_r + \frac{d\phi}{dt} + j\omega_r \varnothing_r \tag{9}$$

$$\varnothing_s = \mathrm{L_s i_s} + \mathrm{L_m i_r} \tag{10}$$

$$\varnothing_r = L_m i_s + L_r i_r \tag{11}$$

The equivalent two-phase model of the symmetrical variable speed wind turbine (dq frame) used to synchronously rotating reference frame (dq frame) as follows [7]:

$$v_{sd} = R_s \cdot i_{sd} + \frac{d\phi_{sd}}{dt} - \omega_s \phi_{sq} \tag{12}$$

$$v_{sq} = R_s \cdot i_{sq} + \frac{d\phi_{sq}}{dt} + \omega_s \phi_{sd} \tag{13}$$

$$v_{rd} = R_r \cdot i_{rd} + \frac{d\phi_{rd}}{dt} - \omega_r \phi_{rq} \tag{14}$$

$$v_{rq} = R_r \cdot i_{rq} + \frac{d\phi_{rq}}{dt} + \omega_r \phi_{rq} \tag{15}$$

The stator and rotor fluxes using the synchronously rotating reference frame (d,q frame) are given as follows [5, 8, 9, 22]:

$$\begin{cases} \phi_{\mathrm{sd}} = \mathrm{L_s i_{sd}} + \mathrm{L_m i_{rd}} \\ \phi_{\mathrm{sq}} = \mathrm{L_s i_{sq}} + \mathrm{L_m i_{rq}} \end{cases} \tag{16}$$

$$\begin{cases} \phi_{rd} = L_r i_{rd} + L_m i_{sd} \\ \phi_{rq} = L_r i_{rq} + L_m i_{sq} \end{cases} \tag{17}$$

where R_s, R_r indicate equivalent resistance of stator and rotor windings. L_s, L_r, L_m indicate self and mutual inductances of stator and rotor windings, respectively. Ignoring the power losses in the stator and rotor resistances, the active and reactive powers from the stator are given by

$$P_S = \frac{3}{2}\left(v_{sd} \cdot i_{sd} + v_{sq} i_{sq}\right) \tag{18}$$

$$Q_S = \frac{3}{2}\left(v_{sd} \cdot i_{sd} - v_{sq} i_{sq}\right) \tag{19}$$

$$P_r = \frac{3}{2}\left(v_{rd}.i_{rd} + v_{rq}i_{rq}\right) \tag{20}$$

$$Q_r = \frac{3}{2}\left(v_{rd}.i_{rd} + v_{rq}i_{rq}\right) \tag{21}$$

The electromagnetic torque is given by [4, 5, 22, 26]:

$$T_e = \frac{3}{2}p\phi_s i_{sq} = -\frac{3}{2}p\phi_s \frac{L_m}{L_s} i_{rq} = -\frac{3}{2}p\frac{V_{sq}}{\omega_s}\frac{L_m}{L_s} i_{rq} \tag{22}$$

The synchronous model is also expressed in the (d,q) synchronous Park's model, and the voltage equations of the PMSG are represented as follows [7]:

$$\frac{di_{sd}}{dt} = \frac{1}{L_d}\left(-R_s i_{sd} + \omega L_q i_{sq} - V_{sd}\right) \tag{23}$$

$$\frac{di_{sq}}{dt} = \frac{1}{L_q}\left(-R_s i_{sq} - \omega_e L_d i_{sd} - V_{sq} + \omega_{PM}\varnothing_f\right) \tag{24}$$

where V_{sd}, V_{sq}, i_{sd} and i_{sq} are voltage and current for the d,q axis of the stator side. $\varnothing_f$ is the magnitude of the flux linkages by using the permanent magnetic flux [Web]; ω_{PM} is the value as rotating speed [rad/s] of the PMSG. The electromagnetic (EM) torque in the rotor could be expressed as follows [7]:

$$T_e = \frac{3}{2}\, p\, \varnothing_f i_{sq} \tag{25}$$

p is the number of pole pairs in the PMSG.

3. Modeling and control of the grid connected to various ESSs

Energy storage systems (ESSs) have a function of converting electrical energy from a power system network into a form that can be stored for converting back to electrical energy when needed [8, 9]. ESS has numerous applications including portable devices, smart grid, building integration, energy efficiency, transport vehicles, and stationary renewable energy resources [27]. In this chapter, only three different distributed ESSs for renewable generation systems were introduced as battery, super capacitor, and electrical dual layer capacitor [23]. **Table 2** summarizes the characteristics of three different ESSs.

3.1. Modeling and control of energy storage systems

Figure 2 shows that each E-ES, for this study, consists of an energy source bank, an inductance and a two-quadrant DC/DC converter connected to the DC link. It also describes how the controller of the DC/DC buck-boost mode generates the gate signals for gate 1 and gate 2 [23].

Categories	ESS Technology	Energy Related Cost ($/kwh)	Replacement Cost ($/kwh)	Energy Function	Charge (response) Time	Efficiency (%)
Chemical Energy Storage	Lead Acid B ESS	300	300	$E(t) = E_0 + \int v(t) \cdot i(t)dt$	1 min to 3 hours	60~70%
	Lion and NaS B ESS	500	500			70~80%
Magnetic Energy Storage	SC and EDLC ESS	30,000	0	$E(t)=\frac{1}{2} \cdot CV^2_{sc\ or\ EDLC}$	1 s to 1min	70~80%

Table 2. Properties of three different ESSs [23].

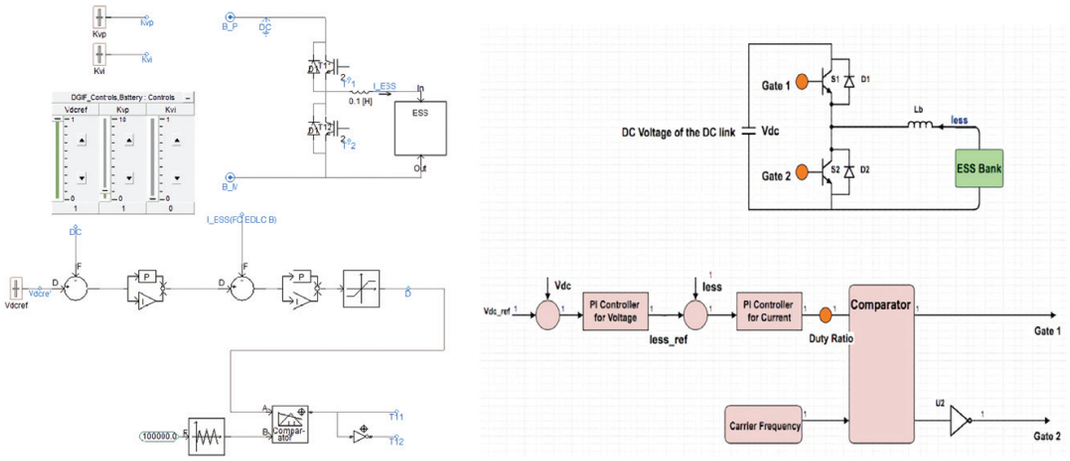

Figure 2. Block diagram of the ESS in PSCAD/EMTDC: modeling of ESS (upper) [14] and controller of ESS (lower) [29].

The reference value of the i_{ess} can be made by using a voltage feedback control between $V_{dc\text{-}ref}$ and V_{dc} with PI controller of the voltage. It can be expressed as follows [2, 25, 28]:

$$i_{ess\text{-}ref} = \left[k_{vp} + \frac{k_{vi}}{s}\right]\left(v_{dc\text{-}ref} - v_{dc}\right) \tag{26}$$

The inner current control loop using a PI controller of current can be produced by using the duty ratio to generate the gate-signal $i_{ess\text{-}ref}$, as given by Eq. (27) [2, 25, 28]:

$$D = \left[k_{bp} + \frac{k_{bi}}{s}\right]\left(i_{ess\text{-}ref} - i_{ess}\right) \tag{27}$$

Finally, the gate signal is generated by comparing the difference between the duty ratio and the carrier frequency.

3.2. Energy flow and Total harmonic distortion of various energy storage systems

The HYESS which is applied to the VSWT system uses DC-DC converters with controller of the ESS illustrated in **Figure 2**. When active power of DFIGs and PMSGs in the rotor side (Pr) or

stator side (Ps) is greater than active power of DFIG and PMSG on the grid side (Pg), the ESS charges the energy flow from the DC bus to the ESS Bank through the S1 switch and S2 diode [26, 29, 30].

Therefore, the source of ESS works to absorb active power from the DC voltage, while acts as a step-down converter when V_{ess} boosts. The DC-DC converter design used as a buck converter circuit, and then D1 (duty ratio) of S1 in the buck mode can be computed by (28) [31]:

$$D1 = [V_{ess}/V_{dc}] \tag{28}$$

When Pg is bigger than Pr, the E-ES energy discharges through S1 and S2, and energy flows to the DC bus (V_{dc}) [27–29]. In this case, the converter acts as a boost converter mode [27–29]. The ESS bank serves as a source to supply active power, which results in the decrease of the voltage V_{ess}. The duty ratio D2 of S2 in the boost mode can be expressed as (29) [25]:

$$D_2 = 1 - D_1 \tag{29}$$

Table 3 summarizes the energy flow in the two modes, that is, buck and boost modes.

The harmonic distortion of the voltage and current waveforms is generally expressed in terms of the fundamental frequency [32]. Power injection from the HY ESS affects the power quality, which is described as voltage and current THD. In Ref. [30], the practices and requirements for harmonic control in electrical power systems are established. **Figure 3** shows the PSCAD/EMTDC modeling for the voltage (Vg), current (Ig), and active power (Pg) of the THD measurement at the point of common connection (PCC) in the proposed system. With the increasing use of the nonlinear devices, harmonic distortion of the voltage waveform is a problem which is receiving the considerable attention. Any periodic waveform of nonsinusoidal form can be synthesized by expressing it as the sum of a series of harmonics of the fundamental frequency by using Fourier analysis (30) [31]:

$$f(t) = a_0 + a_1 \cos \omega t + a_2 \cos 2\omega t + a_3 \cos 3\omega t + \ldots + b_1 \cos \omega t + b_2 \cos 2\omega t + b_3 \cos 3\omega t + \ldots \tag{30}$$

where

$$a_0 = \frac{1}{T}\int_0^T f(t)dt, \quad a_n = \frac{2}{T}\int_0^T f(t)\cos n{\cdot}\omega t{\cdot}dt, \quad b_n = \frac{2}{T}\cdot\int_0^T f(t)\sin n{\cdot}\omega t{\cdot}dt$$

Energy flow	Charge (Pr or Ps > Pg): From DC bus to the ESS	Discharge (Pr or Ps < Pg): From ESS to DC Bus
Bank	Sink as absorb active power	Source as supply active power
V_{ess}	Increase	Reduce
Switch direction of two quadratic converters	S1 switch and S2 diode	S2 switch and S2 Diode
Converter act as	Buck converter as V_{dc}→reduce	Boost converter as V_{dc}→increase

Table 3. Energy flow of the energy storage systems.

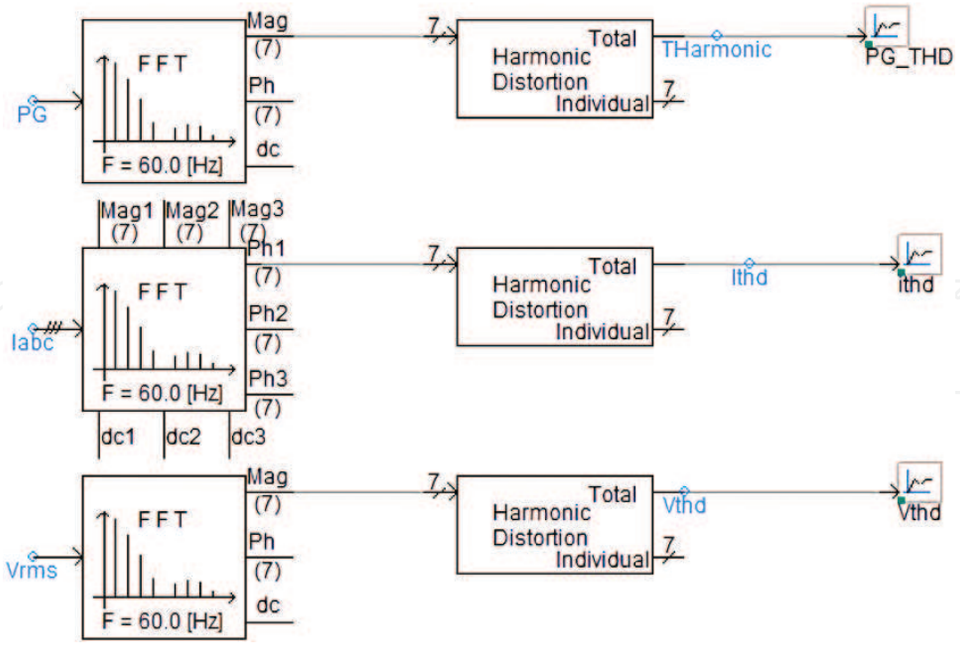

Figure 3. PSCAD modeling of 7th order 60 Hz for THD of active power, current, voltage at the PCC.

Total harmonic distortion (THD) is usually expressed as a percentage of fundamental voltage by the expression as (31):

$$\sqrt{\sum_{n=2}^{n=7}\left(\frac{V_n}{V_1}\right)^2} \times 100\% \tag{31}$$

where V1 = fundamental frequency voltage component, Vn = nth harmonic voltage component.

3.3. Battery energy storage systems (B-ESS)

Batteries have been widely used in many fields, which are referred to as electrical energy storage system, which accumulate electric energy in electrochemical form and delivers direct current (DC). The promising battery which is used as energy storage devices is lithium ion (Li-ion) battery. Due to high electrical potential and energy density of battery, Li-ion batteries are one of the promising solutions for the storage compared to other battery options. In addition, Li-ion batteries do not have poisonous metals (lead, mercury, or cadmium) and memory effect. The main disadvantage of Li-ion battery is the required high production cost [33]. The energy of battery could be calculated by (32):

$$E = IVh \tag{32}$$

where I (A) and V(V) are current and voltage of battery and h (hours) is the charging time. For this study, a Panasonic LJ-SK84A Li-ion storage battery system [34] is used to design about the modeling for the PSCAD battery as 8 KWh from 110 to 165 V in **Figure 4**.

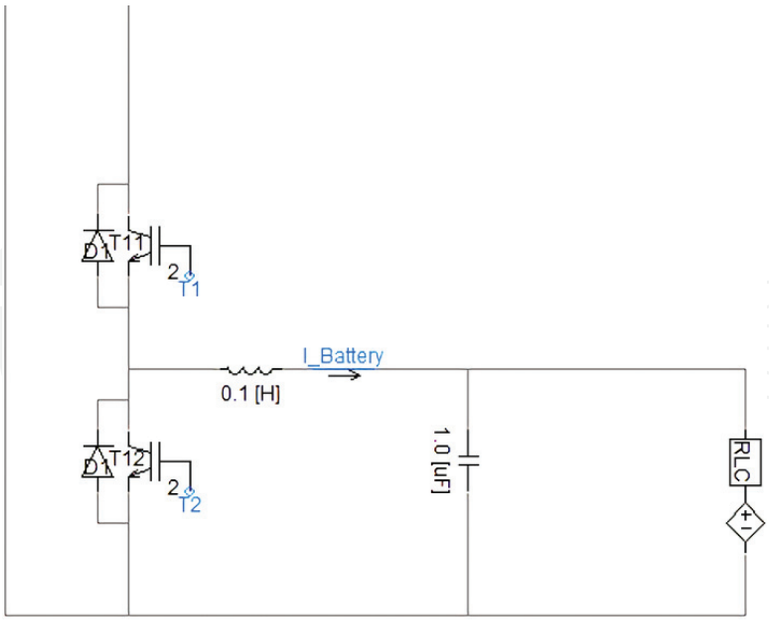

Figure 4. Modeling of PSCAD/EMTDC: BESS.

3.3.1. State of charge

In the Li-ion battery, over charging or over discharging could result in reducing the battery stack life and indirectly increasing the cost. However, accurate calculation of the state of charge (SOC: %) for battery ESS is essential for the battery outputs in powered system that aims at maximizing energy storage system's performance, extending battery life, and realizing the safe operation of the systems including EV, renewable generation, and building integration.

The SOC of the battery is defined as the ratio of the remaining capacity ($Q_{present}$) to the nominal capacity of the cell ($Q_{nominal}$). It could be described as (33)

$$\text{SOC}\ (\%) = \frac{Q\text{-}present}{Q\text{-}nominal} \tag{33}$$

Q is usually measured in the unit of Ah or mAh.

The battery state of charge (SOC) estimation could be calculated by the Coulomb counting (CC) method through the integration of measured battery current or open circuit voltage (OCV) [35–37]. However, unknown initial SOC which caused by the measurement errors and noise in real practice can affect performance, which means unreliable SOC value results in reduced performance and potential risk to the battery system. Therefore, it is critical to develop algorithms that can estimate accurate SOC to improve the performance for the battery energy storage. There are several advanced methods which can be closer to true values over time to compensate for nonlinearity such as extended Kalman filter (EKF) and sigma-point (unscented) Kalman filter (SP/UKF) [35–37].

3.4. Super capacitor ESS

Figure 5 describes about the super capacitors (SCs), which have higher power density, higher round trip efficiency, longer life cycle life, and lower capital cost per cycle than batteries [9, 37]. Therefore, SC is a good candidate for short-term storage (i.e., seconds to minutes). Assuming the initial voltage across the super capacitor (C_{sc}) is V_{sc} (0) after charging for a period t, the instantaneous voltage across the capacitor V_{sc} is given by (34)

$$V_{sc}(t) = V_{sc}(0) + \frac{I_L \cdot t}{C_{sc}} \tag{34}$$

where I_L is the load current entering the capacitor from the unregulated power supply.

3.5. Electrical dual layer capacitor ESS

Capacitors composed of two conducting plates, which are separated by an insulating material [8, 29]. Conventional capacitors store little energy due to the limited charge storage areas and the separation distance between the two charged areas and the separation distance between the two charged plates [29, 38]. However, super capacitors based on the EDL mechanism can store significantly more energy because of the large interface area and the atomic range of charge separation distances [8]. A simple resistive capacitive equivalent circuit of the EDLC-cell is designed in PSCAD/EMTDC as shown in **Figure 5**.

4. Simulation results and discussion

Case I—Analysis of the Variable Speed Wind Turbines with Various ESSs for Power Quality in terms of THD (%).

The simulation results in Case I verify the performance of the hybrid ESS-VSWT by using the PSCAD design tool in terms of the THD (%). The mean wind speed is to make realistic results by using the PSCAD/EMTDC with random noise components during 60 s in **Figure 6**.

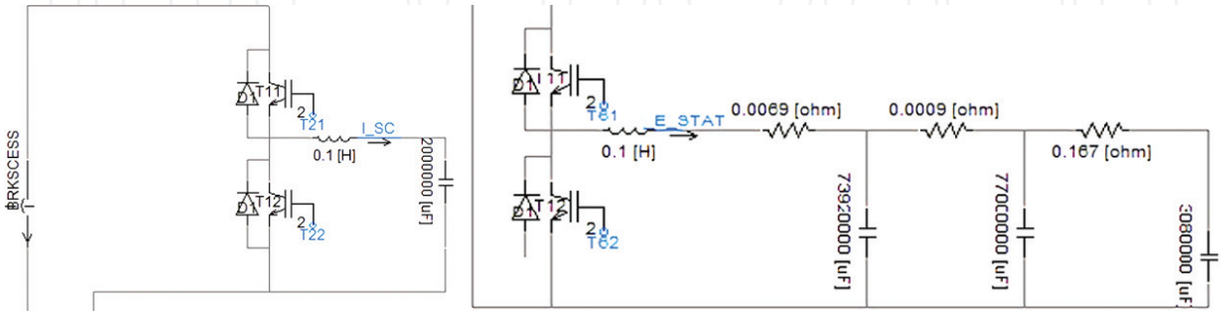

Figure 5. PSCAD modeling of the super capacitor as 2F and EDLC [9, 39].

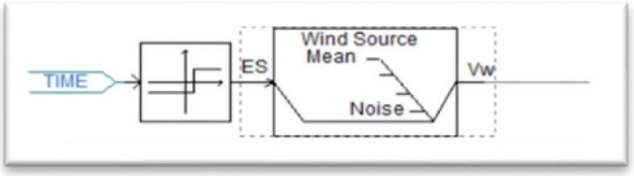

Wind Source	
# of noise components	50
Noise Amplitude controlling Parameter	1 rad/sec
Surface Drag Coefficient	0.0192
Turbulence Scale	600 [m]
Random seed Number (1-99)	3
Time Interval for Random Generation	4 [s]

Figure 6. PSCAD modeling and noise component for the mean wind speed (10 m/s).

Comparison of THD (%) with the HY ESS-VSWT (2 MW, 60 Hz, 10 m/s with random noise) during 60 s

	DFIG			PMSG		
	Avg THD for P	**Avg THD for I**	**Avg THD for V**	**Avg THD for P**	**Avg THD for I**	**Avg THD for V**
No ESS	3.61	6.90	9.73	14.12	4.38	7.37
B- ESS	2.90	4.44	4.58	11.31	2.78	4.94
SC-ESS	2.77	5.68	4.65	10.97	2.30	3.73
E- ESS	2.83	5.65	4.7	11.14	2.78	5.00
B-SC ESS	2.90	5.74	4.43	11.18	1.82	4.96
B- E ESS	2.89	5.75	4.69	11.14	2.79	4.93
SC-E ESS	3.02	5.73	4.60	11.23	2.77	3.71
B-SC-E ESS	3.05	6.06	4.60	1.42	1.82	3.71

Table 4. Comparison of THD at the PCC.

Power quality issue could be verified by the THD which was monitored at the point of common coupling (PCC) in the VSWT-HYESS as illustrated in **Figure 1**. The data (THD: %) in **Table 4** were extracted from using excel file and then taking an average value (THD: %) during 1 min.

4.1. The case of the DFIG-HYESS

Figure 7 describes average THD (%) of a DFIG at the PCC for P, I, and V during 60 s. **Table 5** shows that average THD (%) of the DFIG is a greater than other DFIG-HYESS. This result showed that the proposed HY ESS-DFIG could improve the power quality by reducing the THD. SC-ESS (2.77%), B-ESS (4.4%), and B-SC ESS (4.43%) are the best choices to enhance power quality in the system, as shown in **Figure 8**.

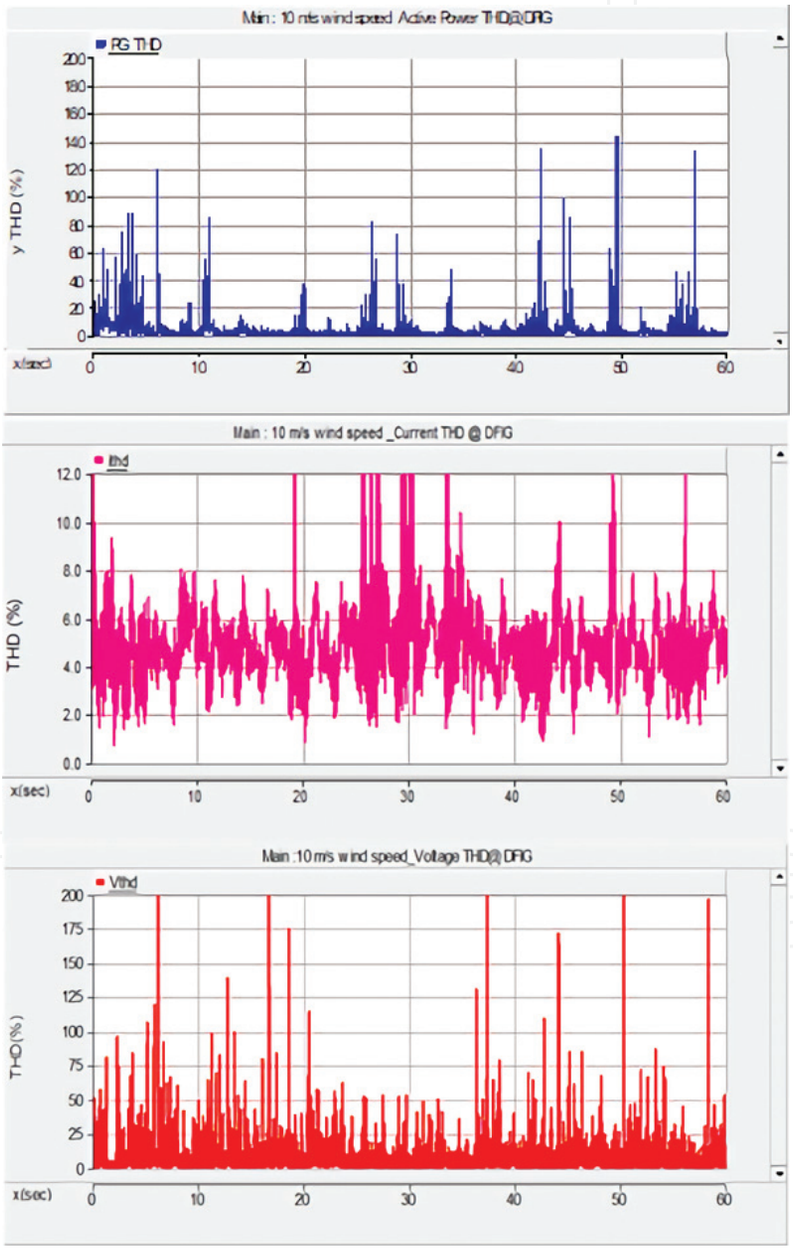

Figure 7. THD (%) of only DFIG during 60 second: active power THD (Pthd: upper), current THD (ithd: middle), voltage THD (Vthd: lower).

Item	Cost ($)
Overnight cost of DFIG	2949000.00
Pb battery ESS	16862.66
Li-ion battery ESS	11992.85
Super capacitor ESS	5574125.98

Table 5. Cost of 1.5 MW Wind Turbine [9].

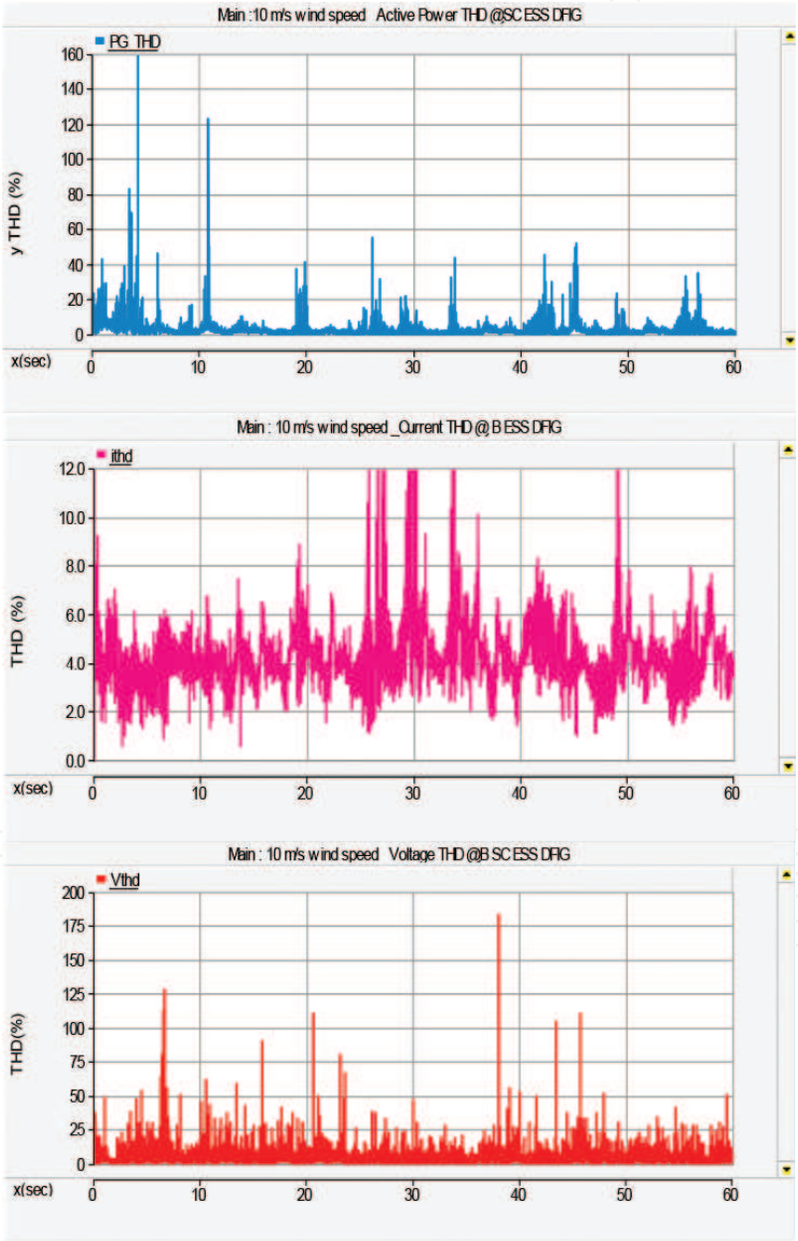

Figure 8. THD (%) of HY ESS DFIG during 60 secs: active power THD of SCESS, current THD of BESS, voltage THD of B-SC-E ESS.

4.2. In the HYESS-PMSG

Table 5 shows that the average THD of PMSGs is bigger than HY ESS-PMSG. These results indicate that an ESS which reduces THD (%) is to be improved. SC-E-B ESS is the most effective option in reducing THD for the voltage (3.71%), current (1.82%), and active power (1.42%), as shown in **Figures 9** and **10**.

Case II– Financial analysis of the DFIG with two ESSs in terms of the payback time ($)

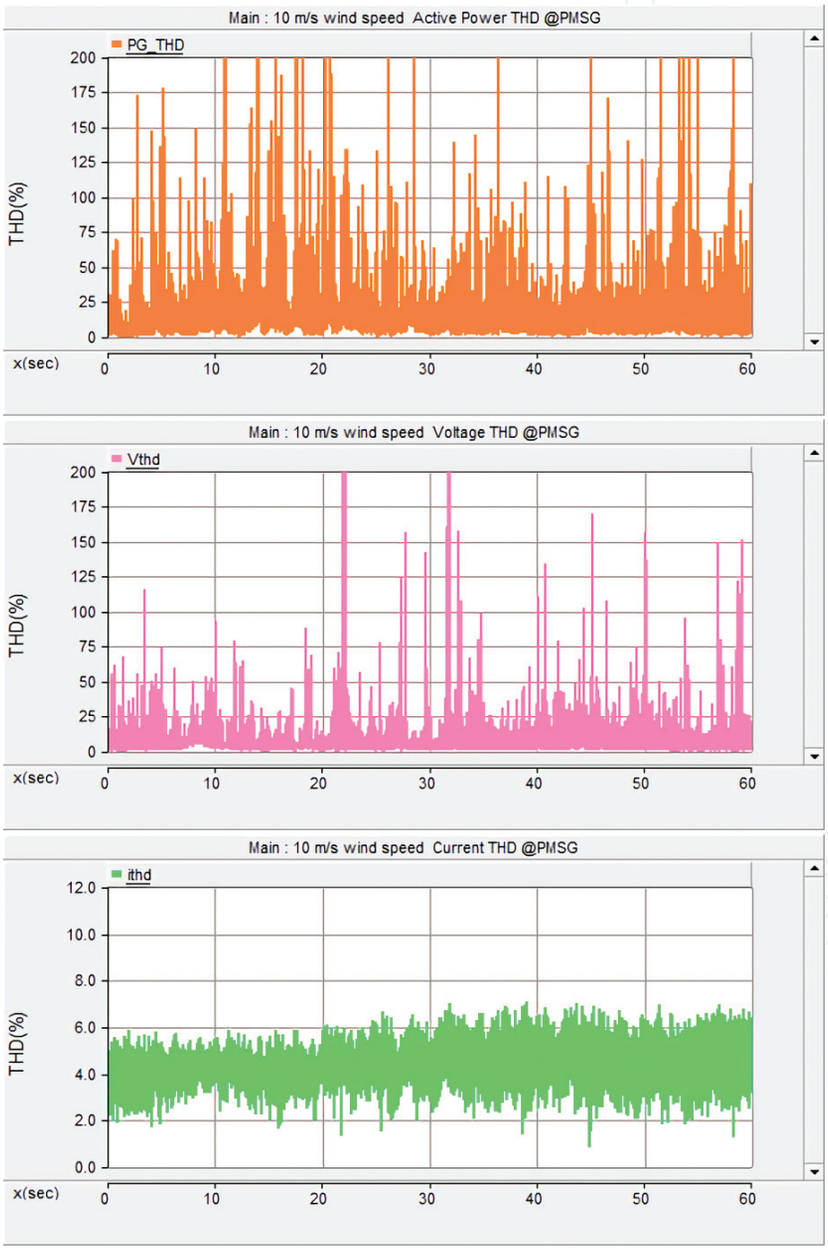

Figure 9. THD (%) of only PMSG during 60 s: active power THD (Pthd: upper), current THD (ithd: middle), and voltage THD (Vthd: lower).

Wind energy is free. However, financial analysis can be used to assess wind project investments such as how to screen cost and the benefits of the project. Regarding the financial analysis, the payback time depends on the amount of time to evaluate the performance of different ESSs such as super capacitor ESS (SCESS), battery ESS (BESS). Payback time is the time in which investors can recover all their investment. It depends on several factors such as O&M, inflation, and depreciation. It will show whether a project is worth establishing the investment to escape the risk. Shorter payback time indicates a more economical project. A 1.5 MW wind generator, which sells the electricity generated to utilities, can serve as an example. There are several manufacturers who provide large capacity DFIG. Generally, the overnight

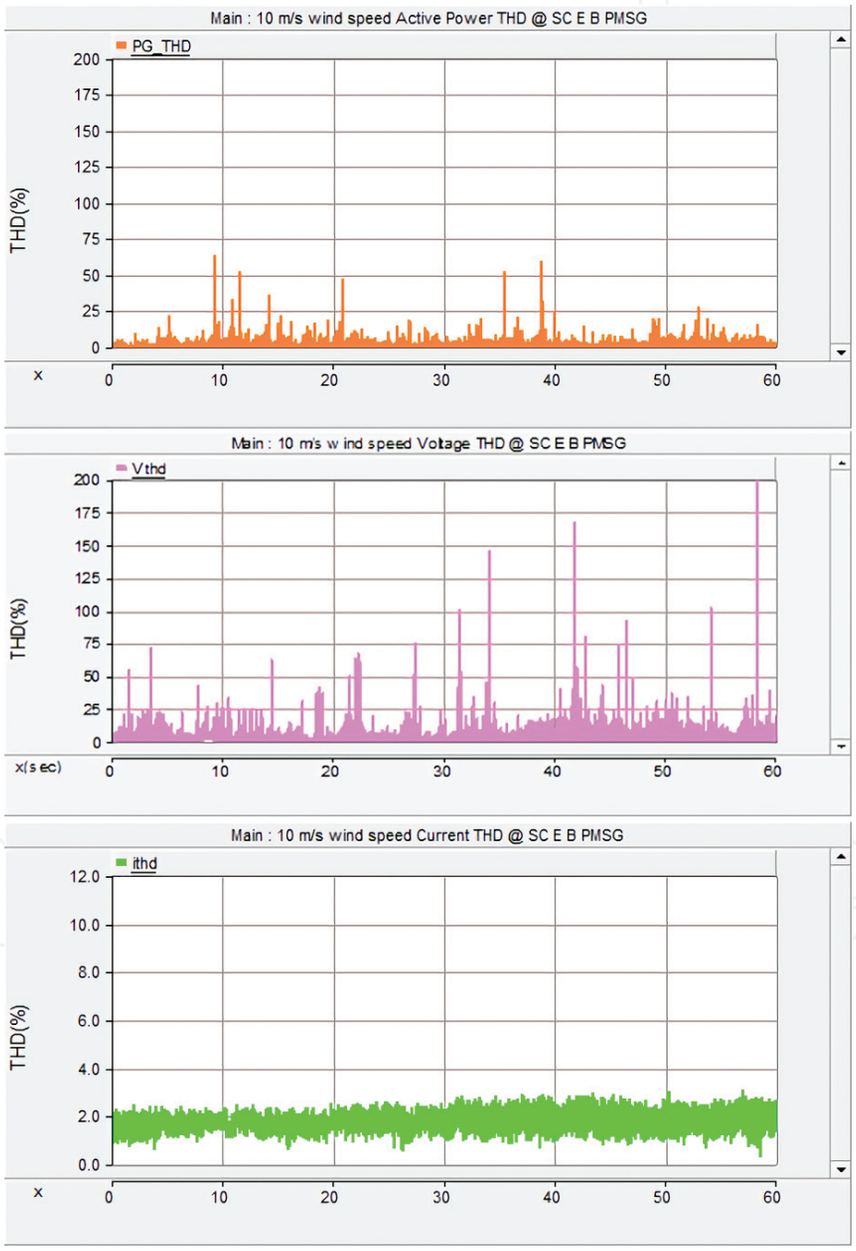

Figure 10. THD (%) of HYESS PMSG during 60 sec: active power THD of B-SC-E ESS, current THD of B-SC-E ESS, voltage THD of B-SC-E ESS.

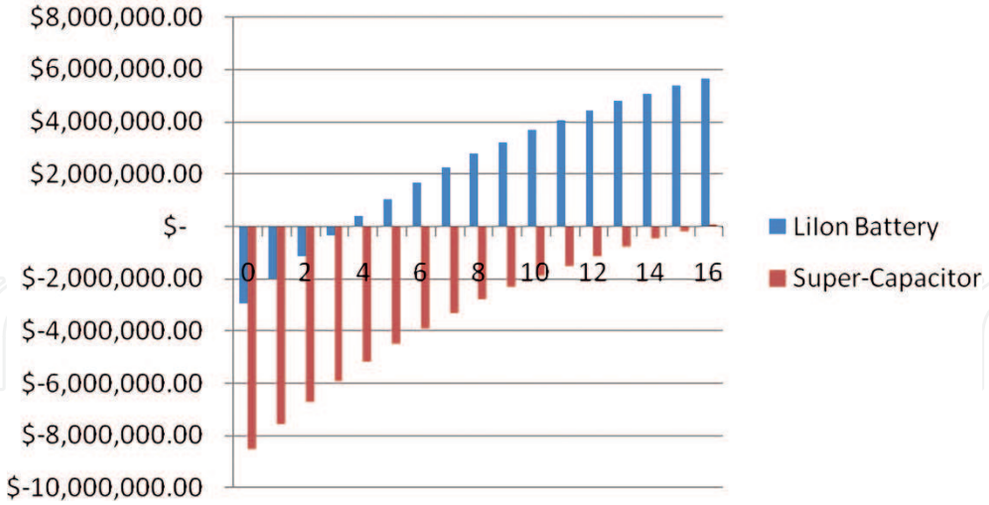

Figure 11. Accumulated cash flow.

cost of a wind generator is $1966/kW. The Cost of O&M per year was assumed as $30.98/kW-Year for this work to find payback time from the [39]. A 83.33 kWh super capacitor ESS and Li Ion battery are chosen [40, 41]. The discount rate is also assumed as 9%. The capital cost of a wind generator is provided in **Table 5**.

Payback time in terms of accumulated cash flow could be expressed as (35)

$$\left(\frac{1}{1+Discount\quad Rate(0.9\%)}\right)^{year} = \text{Capital}\quad \text{Cost} + \text{Net Annual Saving}\ (1,032,838.80) \qquad (35)$$

where capital cost is total overnight cost of DFIG ($) + cost of Li ion or SC ESS. The payback time for DFIG with Li ion ESS is 3.47 years; however, the payback time for DFIG with super-capacitor is 15.76 year as shown in **Figure 11**. If a hybrid ESS (B-SC) ESS is chosen, the payback time will be between 3.47 and 15.76 years, according to the proportion of BESS and SCESS given in this system.

5. Conclusion

This section analyzes the ability of various HY ESSs based on VSWTs to improve power quality in terms of THD under the same situations: three-phase voltage sources used at 20 kV, 60 Hz, 0.04 H, and 2.5 Ω. From the previous results, HYESS-VSWT has been verified to increase the power quality by reducing THD. SC-ESS (2.77%), B-ESS (4.4%), and B-SC ESS (4.43%) of the DFIG's case would be a better option to improve power quality for active power, voltage, and current, respectively, compared to other cases. In the case of the PMSGs, SC-E-B ESS indicated as the best option to reduce THD for voltage (3.71%), current (1.82%), and active power (1.42%). Compared to average active power THD of a DFIG as 3.61% and PMSG as 14.42% without ESS, a THD (%) for PMSG has lower power quality difference output as 10.81% compared to THD (%) of DFIG. This might be a converter configuration issue because

DFIGs are partially controlled by the back-to-back converter such as RSC and GSC, while PMSGs are directly connected through the back-to-back converter to the grid, which make 100% power rated. Regarding average THD, the PMSG-B E SC-ESS as 1.4% has the most outstanding output results compared to other options. Furthermore, the best option's values from the simulation results satisfy the IEEE Standard requirements, which should be less than 4% for current THD and 5% for voltage THD [30].

In addition, a DFIG with various ESSs is a financially attractive option if a chemical battery ESS is used. The payback time is acceptable, and it still has a benefit for the environment. If the new energy storage technology as a super capacitor is considered, the payback time right now is relatively long. However, if there is a technology breakthrough, the cost of a super capacitor will probably decrease and finally be financially attractive. Presently, a hybrid system will still be relatively affordable. This financial forecast helps achieve the high-power quality and reasonable payback time during the short period.

Author details

Youngil Kim[1]* and Robert J. Harrington[2]

*Address all correspondence to: yikim01@gwmail.gwu.edu

1 Green Technology Center, Seoul, South Korea

2 The George Washington University, Washington, D.C., USA

References

[1] US Department of Energy. Annual Energy Outlook 2009 with Projections to 2030. DOE/EIA- 282(2009). March 2009

[2] Mohd. Hasan Ali. Wind Energy Systems Solutions for Power Quality and Stabilization. CRC Press; 2012. Print ISBN: 978-1-4398-5614-7

[3] Anaya-Lara O, Jenkins N, Ekanayake J, Cartwright P, Hughes M. Wind Energy Conversion: Modeling and Control: Wiley. ISBN: 978-0-470-71433-1; August, 2009. 288 pp

[4] Mohd. Abdus Salam. Fundamental of Electrical Machines. 2nd ed: Alpha Science International Ltd. ISBN: 978-81- 8487-163-0; 2013. p. 416

[5] Kirtley JL. Electric Power Principles: Sources, Conversion, Distribution and Use. ISBN: 978-0-470-68636-2. September 2010: Wiley. pp. 159-163

[6] Li H, Chen Z. Overview of different wind generator systems and their comparisons. IET Renewable Power Generator. Jun 2008;**2**(2):123-138

[7] Jayalakshmi NS, Gaonkar DN, Sai Kiran Kumar K. Dynamic modeling and performance analysis of grid connected PMSG based variable speed wind turbines with simple power conditioning system. 2012 IEEE, International Conference on Power Electronics, Drives and Energy Systems. December 16-19, 2012, Bengaluru, India

[8] Muyeen SM, Takahashi R, Murata T, Tamura J. Integration of an energy capacitor system with a variable-speed wind generator. IEEE Transactions on Energy Conversion. Sep 2009; **24**(3):740-749

[9] Kim Y, Zhao J, Harrington RJ. Performance analysis of energy storage systems connected to a doubly fed induction generator. Green Energy and Systems Conference (IGESC), Long Beach, CA, 2015 IEEE, 9-9 Nov. 2015. pp. 30-34. DOI:10.1109/IGESC.2015.7359387

[10] Li S, Haskew TA, Swatloski RP, Gathings W. Optimal and direct-current vector control of direct-driven PMSG wind turbines. IEEE Transactions on Power Electronics. May 2012; **27**(5):2325-2337

[11] Yao DL, Choi SS, Tseng KJ, Lie TT. A statistical approach to the design of a dispatchable wind power-battery energy storage system. IEEE Transactions on Energy Conversion. Dec 2009;**24**(4):916-925

[12] Bludszuweit H, Domínguez-Navarro JA. A probabilistic method for energy storage sizing based on wind power forecast uncertainty. IEEE Transactions on Power Apparatus and Systems. Aug 2011;**26**(3):1651-1658

[13] Mercier P, Cherkaoui R, Oudalov A. Optimizing a battery energy storage system for frequency control application in an isolated power system. IEEE Transactions on Power Apparatus and Systems. Aug 2009;**24**(3):1469-1477

[14] Brekken TKA, Yokochi A, Von Jouanne A, Halamay DA. Optimal energy storage sizing and control for wind power applications. IEEE Transactions on Sustainable Energy. Jan 2011;**2**(1):69-77

[15] Sarrias-Mena R, Fernandez-Ramirez LM, Garcia-Vazquez CA, Jurado F. Dynamic evaluation of two configurations for a hybrid dfig-based wind turbine integrating battery energy storage system. Wind Energy. 2015;**18**(9):1561-1577

[16] Ding M, Chen Z, Su J, et al. Optimal control of battery energy storage system based on variable smoothing time constant. Automation of Electric Power Systems. Jan 2013;**37**(1): 19-25

[17] Teleke S, Baran ME, Bhattacharya S, Huang AQ. Optimal control of battery energy storage for wind farm dispatching. IEEE Transactions on Energy Conversion. Sep 2010; **25**(3):787-794

[18] Abbassi A, Dami MA, Jemli M. Statistical Characterization of Capacity of Hybrid Energy Storage System (HESS) to Assimilate the Fast PV-Wind Power Generation Fluctuations. 2017 International Conference on Advanced Systems and Electric Technologies (IC_ASET), Hammamet, Tunisia, 14-17 Jan. 2017

[19] Bouharchouche A, Berkouk EM, Ghennam T, Tabbache BA. Modeling and control of a Doubly Fed Induction Generator with Battery-Supercapacitor Hybrid Energy Storage for Wind Power Applications. In: Proc. POWERENG. 2013. pp. 1392-1397; 2013

[20] Luo W, Feng S, Ge W, Wang Z. Research on the control strategy of large-scale wind power energy storage system. IEEE Innovative Smart Grid Technologies. 2012:1-4, 2012

[21] Li J, Bi J, Yan G, Ge Y, Jin P. Research on improving power quality of wind power system based on the flywheel energy storage system. 2016 China International Conference on Electricity Distribution (CICED), 10-13 Aug 2016, Xi'an, China

[22] Ghennam T. Berkouk EM, Bruno F. Modeling and control of a doubly fed induction generator (DFIG) based wind conversion system power engineering, energy and electrical drives. 2009. POWERING09, pp. 507-512, Lisbon, 18-20 March 2009

[23] Kim Y, Harrington R. Analysis of various energy storage systems for variable speed wind turbines. IEEE Conference on Technologies for Sustainability – Engineering and the Environment (SusTech 2015), July 30-Aug 1, 2015 in Ogden, Utah

[24] Abad G, Lopez J, Rodriguez M, Marroyo L, Iwansk G. Doubly Fed Induction Machine: Modeling and Control for Wind Energy Generation. John Wiley & Sons; Sep 28, 2011

[25] Mohan NED. Power Electronics: A first Course. ISBN-13: 978-1118074800

[26] Lipo TA. Analysis of Synchronous Machines. 2nd ed: CRC Press; 2012

[27] Kalbat A. PSCAD simulation of grid-tied photovoltaic systems and Total Harmonic Distortion analysis. EPECS – 2013. pp. 1-6; 2013

[28] Jiang Z, Yu X. Modeling and control of an integrated wind power generation and energy storage system. Proc. Power Energy Soc. General Meeting. pp. 1-8. 2010-Jul-2630

[29] Qu L, Qiao W. Constant power control of DFIG wind turbines with super capacitor energy storage. IEEE Transactions on Industry Applications. January/February 2011;**47**(1)

[30] IEEE-std-519-1992

[31] Bollen MHJ. Understanding Power Quality Problems – Voltage Sags and Interruptions. John Wiley & Sons. ISBN: 0-7803-4713-7

[32] Arrillaga J, Watson NR. Power System Harmonics. 2nd ed; November, 2003. ISBN: 978-0-470- 85129-6. 412 pp

[33] Chakraborty S, Simoes MG, Kramer WE. Power Electronics for Renewable and Distributed Energy Systems: A Sourcebook of Topologies, Control and Integration. Springer-Verlag London: Springer. ISBN 978-1-4471-5103-6; 2013

[34] Panasonic Energy Solutions - Residential Storage Bat- Tery System, Panasonic Corporation; 2015

[35] Plett GL. Extended kalman filtering for battery management systems of LiPB-based hev battery packs, part 1. Background. Journal of Power Sources. 2004;**134**:252-261

[36] Plett GL. Extended kalman filtering for battery management systems of LiPB-based hev battery packs, part 2. Modeling and identification. Journal of Power Sources. 2004;**134**: 262-276

[37] Plett GL. Extended Kalman filtering for battery management systems of LiPB-based HEV battery packs part 3. State and parameter estimation. Journal of Power Sources. 2004; **134**:277-292

[38] Manitoba HVDC Research Center, https://hvdc.ca/pscad/

[39] Zhai Q et al. Cost benefit analysis of using clean energy supplies to reduce greenhouse gas emissions of global automotive manufacturing. Energies 4.10 (2011): 1478-1494

[40] Babazadeh H, Gao W, Wang X. Controller design for a hybrid energy storage system enabling longer battery life in wind turbine generators. North American Power Symposium (NAPS), IEEE; 2011

[41] Takahashi R et al. Efficiency calculation of wind turbine generation system with doubly fed induction generator. Electrical Machines (ICEM), 2010 XIX International Conference on. IEEE; 2010

IntechOpen